energies

MDPI

Article

Experimental Study of Horizontal Flow Boiling Heat Transfer Coefficient and Pressure Drop of R134a from Subcooled Liquid Region to Superheated Vapor Region

Ernest Gyan Bediako *, Petra Dančová and Tomáš Vít

Department of Power Engineering Equipment, Faculty of Mechanical Engineering, Technical University of Liberec, 461 17 Liberec, Czech Republic; petra.dancova@tul.cz (P.D.); tomas.vit@tul.cz (T.V.)

* Correspondence: ernest.gyan.bediako@tul.cz; Tel.: +420-776-037-976

Abstract: For the past few years, research in the field of flow boiling heat transfer has gained immense popularity for unravelling the dominant mechanism responsible for controlling heat transfer and identifying a parametric trend for understanding the characteristics of flow boiling heat transfer. This has led to several assumptions and models for predicting heat transfer during flow boiling without any known generalized mechanism. This study therefore seeks to experimentally study the characteristics of heat transfer during flow boiling over a wide range but small increase in vapor quality from a single-phase subcooled region through to a two-phase superheated vapor region. The study was performed with an R134a refrigerant in a single horizontal circular stainless-steel smooth tube that had an internal diameter of 5 mm. In this experimental study, local heat transfer coefficients and frictional pressure drop were measured for low heat fluxes of 4.6–8.5 kW/m^2, mass fluxes of 200–300 kg/(m^{2}s), vapor quality from −0.1 to 1.2 and a low constant saturation pressure of 460 kPa. Flow patterns observed during the study were recorded with a high-speed camera at 2000 fps. In covering a wide range of vapor quality, a peak of heat transfer coefficient near a vapor quality of zero and a local minimum observed in the low vapor quality region were observed, and both were sensitive to heat flux and mildly sensitive to mass flux. Generally, at low vapor quality, the heat transfer coefficient deteriorated with vapor quality and this was sensitive to heat flux but insensitive to mass flux and vapor quality, indicating nucleate boiling dominance in low vapor quality regions. In high vapor quality regions, the heat transfer coefficient was sensitive to mass flux and insensitive to heat flux. This indicates the dominance of convective boiling. In the low vapor quality regions, the flow patterns observed were slug and intermittent, while in the high vapor quality region, annular and mist flow patterns were observed. Generally, frictional pressure drop increased with increasing mass flux and vapor quality in the two-phase region.

Keywords: heat transfer coefficient; flow boiling; R134a; convective boiling; nucleate boiling; vapor quality; mass flux; heat flux

Citation: Bediako, E.G.; Dančová, P.; Vít, T. Experimental Study of Horizontal Flow Boiling Heat Transfer Coefficient and Pressure Drop of R134a from Subcooled Liquid Region to Superheated Vapor Region. *Energies* **2022**, *15*, 681. https://doi.org/10.3390/en15030681

Academic Editors: Krystian Czernek, Stanislaw Witczak, Jerzy Hapanowicz and Roman Dyga

Received: 6 December 2021
Accepted: 11 January 2022
Published: 18 January 2022

1. Introduction

Research in the area of flow boiling heat transfer spans over decades [1,2]. This is because flow boiling heat transfer has been identified as an efficient technique for dissipating heat from small diameter tubes, which find their application in compact heat exchangers, air conditioners, refrigeration systems and many more [3,4]. In most of these applications, the flowing refrigerant enters the tube as a subcooled liquid, goes through a saturation phase and exits as a superheated vapor. In this process, three phases are encountered (subcooled phase, saturation phase and superheated vapor phase). Although there have been many studies on flow boiling heat transfer, with the majority of them focusing on the effect of mass flux, heat flux, vapor quality, tube diameter, refrigerant type and saturation conditions (saturation pressure and saturation temperature) [5], there

have been limited studies in the literature that have considered heat transfer characteristics from a subcooled liquid phase, through to two-phase, to a superheated vapor phase in a single experiment [6]. Additionally, many of these studies focus on heat fluxes greater than 5 kW/m^2, vapor qualities between the range of 0–1 and medium to high mass fluxes [7]. According to Smith et al. [8], applications that involve low heat and mass fluxes are being encountered in many fields recently, including refrigerators and plate heat exchangers. Better understanding and accurate prediction of flow boiling heat transfer over a wide range of vapor qualities, from a subcooled region to a superheated vapor region, for low heat and mass fluxes are required for reliable design of systems that operate in such low conditions.

In flow boiling heat transfer, two distinct mechanisms are assumed to control the heat transfer in small diameter tubes: (i) nucleate boiling and (ii) convective boiling [9]. In the case of nucleate boiling, the formation of bubbles at the walls of the tube is assumed to control the heat transfer, whereas conduction and convection through a thin liquid film and evaporation at the liquid–vapor interface are assumed to largely control convective boiling. They can coexist over a wide range of vapor qualities. These mechanisms are related to the heat transfer coefficient, which is mainly influenced by mass flux, heat flux, vapor quality and saturation conditions. When the heat transfer coefficient is not affected by mass flux and vapor quality, but is highly affected by heat flux and saturation pressure, nucleate boiling is assumed to be the predominant mechanism controlling the heat transfer. When the heat transfer coefficient is not affected by heat flux but is highly influenced by mass flux and vapor quality, then convective boiling is assumed to be the dominant mechanism controlling the heat transfer coefficient. There are instances where both mechanisms can coexist. These instances are mostly when the heat transfer coefficient is influenced by heat flux and mass flux over a range of vapor quality [10,11]. The mechanisms that are assumed to control heat transfer during flow boiling are also related to flow patterns in that liquid, and vapor phase distribution significantly affects the observed two-phase flow patterns. Channel size and geometry configuration affect the liquid and vapor phase distribution, which in turn affects the flow patterns and the characteristics of the heat transfer during flow boiling. [12,13]. Despite extensive study in this field, the general characteristics and the dominant mechanism responsible for controlling heat transfer during flow boiling remain unclear and contradicting [14,15].

For example, Tibirica and Ribatski [16] investigated flow boiling heat transfer of R134a and R245fa in a horizontal stainless-steel tube of 2.3 mm internal diameter. Their work evaluated the effect of mass fluxes from 50 to 700 kg/(m^{2}s), heat flux of 5 to 55 kW/m^2, and exit saturation temperatures of 22, 31 and 41 °C on heat transfer coefficients. They considered a vapor quality range of 0.05 to 0.90. They reported that the heat transfer coefficient increases with increasing heat flux, mass flux and saturation temperature. They also reported a distinctive heat transfer behavior for increasing vapor quality below a threshold mass flux of 200 kg/(m^{2}s). They indicated that, irrespective of the mass flux, an increased heat flux resulted in an increased heat transfer coefficient.

Paul et al. [17] recently investigated flow boiling heat transfer in 5 mm smooth stainless steel using R134a as the refrigerant. They considered a mass flux range of 301–800 kg/(m^{2}s), a heat flux of 8.5 kW/m^2 and vapor quality within the range of 0 to 1. Their study observed that the heat transfer coefficient increases with mass flux and vapor quality, with a minor effect of heat flux. They concluded that convective boiling was the dominant mechanism controlling heat transfer.

Xu et al. [3] studied the flow boiling heat transfer coefficient of R134a in three horizontal circular smooth tubes of different diameters. Their study was conducted for a heat flux range of 18–35.5 kW/m^2 and saturation pressure range of 0.578–0.82 MPa. The vapor quality range was between 0.03 and 1.0. Their study concluded that the heat transfer coefficient increased with heat flux and saturation pressure and, thus, nucleate boiling was the dominant mechanism controlling the heat transfer.

Kanizawa et al. [18] also presented a flow boiling experimental study of R134a, R245fa and R600 refrigerants in small diameter tubes of 0.38–2.6 mm. The mass fluxes were varied

from 49 to 2200 kg/(m^{2}s) and heat fluxes up to 185 kW/m^2. They investigated the effects of the experimental conditions on the heat transfer coefficient and dry-out qualities identified. Their study reported that heat transfer coefficient increased with increasing mass flux, heat flux and saturation temperature. They also reported a remarkable increase in heat transfer coefficient, with heat fluxes below a vapor quality of 0.4. They found a negligible effect of saturation temperature at 5 kW/m^2 heat flux. However, at higher heat fluxes, the effect of heat fluxes on the heat transfer coefficient were pronounced. They found that mass flux had a negligible effect on the heat transfer coefficient at vapor qualities below 0.4. However, beyond this vapor quality, increasing mass flux produced an increased heat transfer coefficient.

An interesting study was presented by Lima et al. [19] on R134a flowing in a 13.84 mm internal diameter smooth horizontal copper tube on the heat transfer coefficient. Their study considered vapor qualities that ranged from 0.01 to 0.99, mass flux of 300 and 500 kg/(m^{2}s), heat fluxes of 7.5 and 17.5 kW/m^2 and saturation temperatures of 5, 15, and 20 °C. They observed that the heat transfer coefficient increased with mass flux. However, this increase was pronounced at higher vapor qualities. The heat transfer coefficient increased with higher heat fluxes at lower vapor qualities. This effect, however, decreased as vapor quality increased until a local minimum was reached. The vapor quality at which this local minimum was observed was sensitive to both heat and mass fluxes.

A complete evaluation of the flow boiling phenomena and pressure drop of R134a in a smooth tube of 8.62 mm was presented by Celen et al. [20]. They evaluated the effect of mass flux, saturation temperature and heat flux on the heat transfer coefficient and pressure drop for ranges of 290–381 kg/(m^{2}s), 15–22 °C and 10–15 kW/m^2, respectively. They reported that the heat transfer coefficient and pressure drop were affected by mass fluxes for all conditions investigated. They indicated that at mass flux of 290 kg/(m^{2}s), increasing heat flux led to a higher heat transfer coefficient. However, this effect decreased for a mass flux of 381 kg/(m^{2}s).

Bandarra Filho et al. [21] also performed an experimental study of flow boiling heat transfer and pressure drop on R134a in a horizontal smooth microfin tube. The conditions studied were saturation temperature of 5 °C, vapor quality in the range of 0.005 to 0.9, mass flux in the range of 100–500 kg/(m^{2}s) and heat flux of 5 kW/m^2. They reported that the heat transfer coefficient was negligibly affected by vapor qualities at lower mass fluxes of 150 kg/(m^{2}s). However, at high mass flux, the heat transfer coefficient increases correspondingly.

An experimental investigation by Manavela et al. [22] on the effect of mass flux and heat flux on heat transfer coefficient for a smooth stainless-steel tube with an inner diameter of 5 mm was performed using R134a at 34 °C. They concluded that, at lower vapor qualities, a higher heat flux produced a higher heat transfer coefficient. They also concluded that the effect was more evidenced at lower mass fluxes in that at low mass flux, the effect of vapor quality had no observable effect on the heat transfer coefficient.

Balachander et al. [23] studied flow boiling heat transfer behavior of R134a and R404A at low mass fluxes of 57 and 102 kg/(m^{2}s). Heat fluxes for R134a was between 7.5 to 8.3 kW/m^2, saturation temperatures of −15 to 0 °C and vapor qualities between 0.1 and 1.0. The study was performed in a 7.9 mm tube. Their study revealed that the heat transfer coefficient was a strong function of heat flux and that nucleate boiling was dominant. The heat transfer coefficient decreased with increasing vapor quality and increasing saturation temperature. They reported that the flow pattern observed was stratified wavy.

Another extensive flow boiling heat transfer study was carried out by Saiz Jabardo et al. [24] in a horizontal copper tube of 12.7 mm internal diameter. Their study considered mass flux range of 50–500 kg/(m^{2}s), 5–20 kW/m^2, vapor quality between 0.05 and 1 and evaporating temperatures of 5 and 8 °C. They observed that at low mass fluxes, the heat transfer coefficient did not have significant dependence on vapor quality. Their study also indicated that the heat transfer coefficient even decreased slightly with increasing vapor qualities. The heat fluxes have an effect on the heat transfer coefficient over the entire range of vapor

qualities studied at low mass fluxes. At low vapor qualities and even at higher mass fluxes, heat fluxes had an effect on the heat transfer coefficient. At mass fluxes greater than 200 kg/(m^2s), the heat transfer coefficient increased with increasing vapor quality until dry-out was reached.

From the literature presented above, it is observed that there is a unanimous conclusion on how strongly the heat transfer coefficient depends on mass flux. However, with respect to heat fluxes, saturation conditions and vapor qualities, which most studies considered between 0 and 1, there is no agreement on their effect on the heat transfer coefficient. For example, while Saiz Jabardo et al. [24] reported that increasing vapor quality has a decreasing effect on the heat transfer coefficient, Bandarra Filho et al. [21] reported a negligible effect of vapor quality on the heat transfer coefficient and Manavela et al. [22] reported an ever-increasing effect of vapor quality on the heat transfer coefficient. Additionally, there are less studies for low heat flux conditions below 5 kW/m^2 whose application is increasingly encountered in refrigerators and plate heat exchangers [5].

Interestingly, diverse qualitative flow regime descriptions have been proposed to describe the characteristics of a heat transfer coefficient from a subcooled region to a superheated vapor region. According to Hewitt [25], these qualitative descriptions have been the basis for design calculations, theories and correlations for many years. However, according to Barbosa [26], there have been several disagreements concerning different qualitative descriptions and their actual representation of the heat transfer coefficient for certain regions of flow boiling processes. For example, Collier and Thome [27] proposed a qualitative description of the flow boiling heat transfer coefficient from single-phase all liquid through to two-phase to single-phase all vapor and the mechanisms controlling the heat transfer in different regions.

Figure 1 depicts the variation in the heat transfer coefficient for an increasing heat flux from (i) to (vii), as proposed by Collier and Thome [27]. From their description, at low heat flux, there is a consumption of liquid near the wall region, which takes place at a relatively high quality, resulting in the occurrence of liquid film dry-out. However, at low vapor quality, this occurrence is known as departure from nucleate boiling (DNB). The process of passing through the departure from nucleate boiling, which is known as critical heat flux, is what causes saturated film boiling at high heat fluxes. Kandlikar [28] challenged the descriptive flow regime scheme developed by Collier and Thome [27] in that, according to Collier and Thome [27], the heat transfer coefficient in the region with vapor quality below zero (0) is assumed to be a linear increase. According to Kandlikar [28], the linear increase is not an accurate representation of the heat transfer coefficient in the negative quality region. He also tested the validity of Collier and Thome's [27] schematic representation of heat transfer coefficient from a vapor quality of zero (0) to one (1). He observed that the trend of a constant heat transfer coefficient in the nucleate boiling regime and an ever-increasing heat transfer coefficient with vapor quality for convective boiling is not entirely accurate. For a vapor quality range around and below zero (0), Barbosa, Kandlbinder and Urso [26,29,30] reported an observed sudden rise in heat transfer coefficient, which has been attributed to different theories. They reported that this observation was a deviation from the classical description of the heat transfer coefficient by Collier and Thome and Kandlikar [27–32], upon which many design calculations and formulations of various flow boiling correlations are based.

It can be observed that there is no agreed parametric trend on the effect of heat flux, vapor quality and saturation conditions on the heat transfer coefficient. Most of the studies were centered above a heat flux range of 5 kW/m^2 and between a vapor quality of 0 and 1. Although the qualitative description of Collier and Thome [27] on the heat transfer coefficient covered the entire range of vapor quality from a single-phase liquid region to a superheated vapor region, certain regions have been challenged by other authors to inaccurately represent heat transfer coefficient.

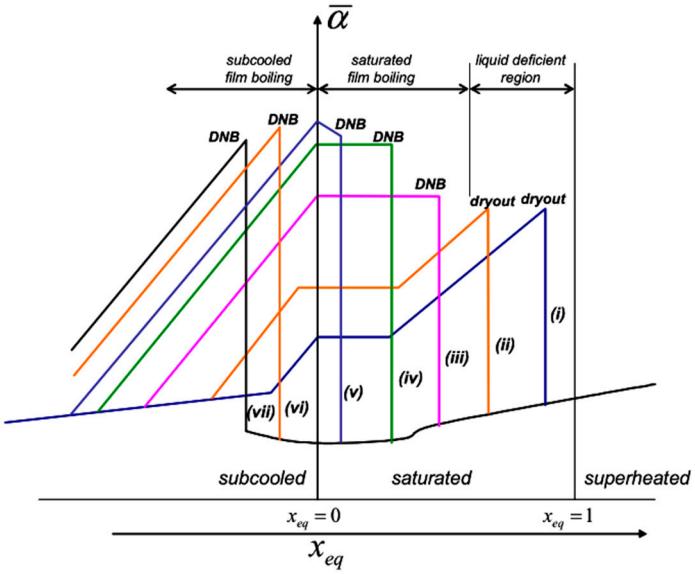

Figure 1. Heat transfer coefficient behavior as a function of vapor quality and heat flux from Collier and Thome [27]. Reproduced from [26], ABCM: 2005.

This study, therefore, tries to narrow this gap by focusing on the heat transfer characteristics, the mechanism controlling heat transfer and the pressure drop of R134a in a single horizontal circular stainless-steel smooth tube, from a subcooled liquid region to a superheated vapor region with a small vapor quality increment for low heat flux and saturation pressure conditions. The wide range of vapor quality from a single-phase subcooled region through to two-phase to a superheated vapor region is scarcely reported in the literature. Flow patterns observed were also recorded to complement the analysis.

2. Experimental Set Up

The experimental studies were carried out at the Norwegian University of Science and Technology's Two-Phase Flow Instability facility, which is part of the Department of Energy and Process Engineering (NTNU). Figure 2 shows the entire experimental facility for this study. It is a closed loop facility made up of a heated section, a conditioner, a pump, a main tank and a visualization glass (shown in Figure 3). The working fluid used was an R134a refrigerant whose inlet temperature was controlled with a shell and tube type heat exchanger. The saturation conditions in the main tank were used to control the fluid pressure in the test section. A Coriolis mass flow meter mounted at the test section's inlet monitored the flow rates. The test section was a stainless-steel tube with an internal diameter of 5 mm and a length of 2035 mm. Figure 4 shows the test section, which is made up of five equal-length subsections that can be heated separately using Joule's effect. A controller and a rectifier circuit were used to convert Alternate Current to Direct Current (AC–DC) power supply to the test section. The total electrical input power was computed using measured voltage and current in the heated region. To reduce heat losses, suitable insulation was used at the outer surface of the test section. How axial heat conduction influences the heated wall was studied in [31]. For measuring temperatures at different locations, ten thermocouples were installed on the outside bottom wall and seven (7) on the outside top wall. Thermocouples were fitted on the top, bottom, and side walls, as well as in-flow internal thermocouples, at positions 1117 and 1917 mm from the inlet. Figure 5 is the simplified P&ID of the experimental test facility, including the R134a refrigerant and the glycol loop as described in Figure 2. At a frequency of 10 Hz, the temperature, mass flow rate, absolute pressures and pressure differential were measured. The LabVIEW National Instrument data collection system was used to record the experimental data.

Figure 2. Experimental facility.

Figure 3. Position of visualization glass tube.

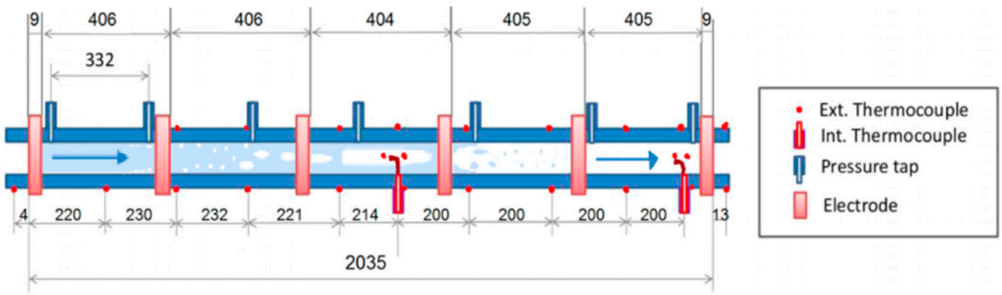

Figure 4. Schematic drawing of heated test session.

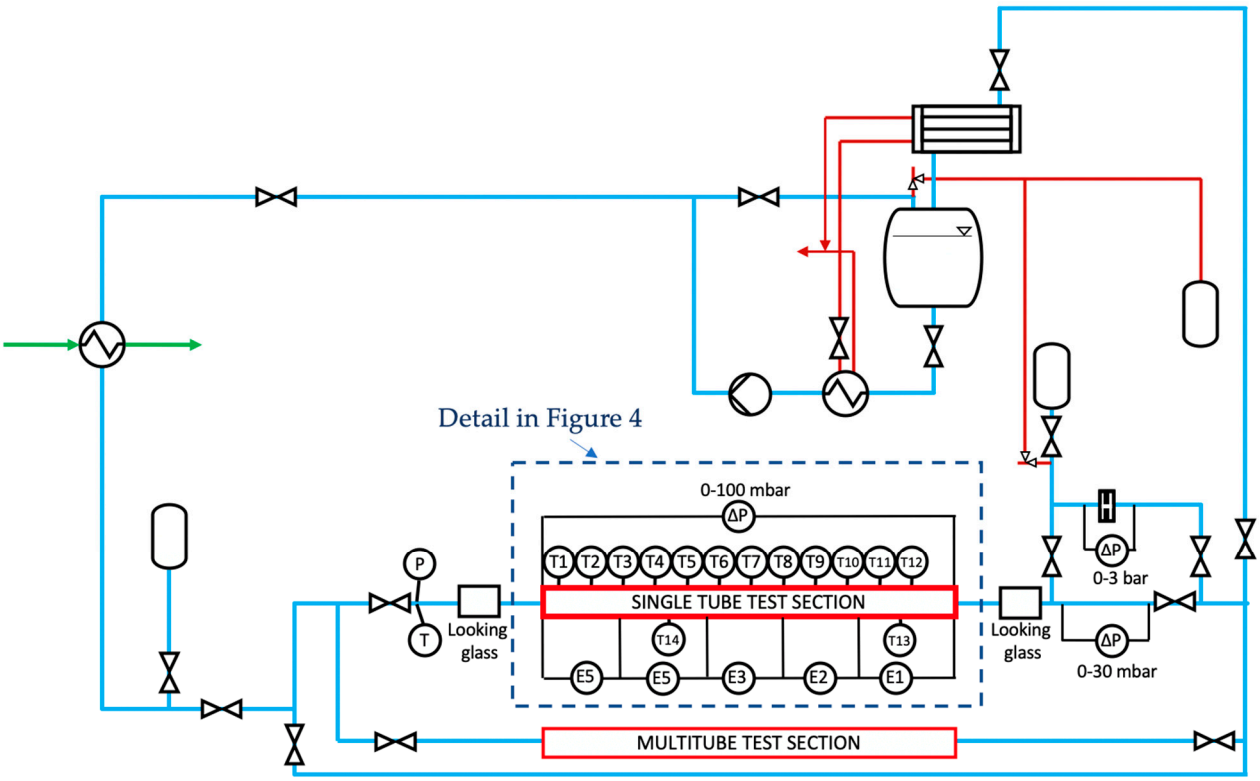

Figure 5. Simplified P&ID of the experimental test facility (main loop), including the R134a refrigerant and the glycol loop as described in Figure 2. T indicates the position of the thermocouples, P indicates the absolute pressure meter, ΔP indicates the differential pressure meter, E indicates the tank.

2.1. Measurement

This work aims to investigate the characteristics of heat transfer coefficient and pressure drop over a wide range but small increase in vapor qualities. As a result, across a wide vapor quality range of −0.1 to 1.2, we measured the heat transfer coefficient and frictional pressure drop for various heat fluxes and mass fluxes. A differential pressure transducer was used to measure the two-phase total pressure drop. The recorded mass flow, temperatures and heat fluxes were used to calculate the heat transfer coefficient and fluid quality. The experimental conditions and thermophysical properties for this study are presented in Tables 1 and 2 below.

2.2. Fluid Temperature

The fluid temperature was measured at three sites: at the heated section's inlet, inside the heated section at two points, and after the heated section. T-type thermocouples with a 0.5 mm diameter were used to measure the temperature. In an ice–water equilibrium mixture and boiling water, all of the thermocouples in the facility were calibrated simultaneously. Table 3 shows a reference thermocouple that has been checked for accuracy. The absolute pressure at the heated section's inlet and outlet was also measured, and this is utilized to determine the saturation temperature of the fluid based on the equilibrium thermodynamic properties computed with REFPROP [32]. Several experiments were carried out throughout the design of the test section to determine the impact of the installed thermocouples on the flow patterns. These experiments were carried out in a 10 mm acrylic pipe with a 1 mm thick penetration to simulate thermocouple disruptions. The flow patterns observed using a high-speed camera indicated that there was no significant effect on the flow pattern [33].

Table 1. Experimental conditions.

Experimental Condition	Mass Flux (G (kg/(m^{2}s))	Heat Flux (q'' (kW/m^2))	Saturation Pressure (P (kPa))
1	200	4.6	460
2	200	8.5	460
3	300	4.6	460
4	300	8.5	460

Table 2. Thermophysical properties for R134a at saturation pressure of 460 kPa.

Properties	Saturation Pressure = 460 kPa
Saturation Pressure	13.150 °C
Liquid Density	1250.0 kg/m^3
Vapor Density	22.397 kg/m^3
Liquid Enthalpy	217.92 kJ/kg
Vapor Enthalpy	406.06 kJ/kg
Liquid Viscosity	2.258×10^{-4} Pa·s
Vapor Viscosity	1.1219×10^{-5} Pa·s
Liquid Conductivity	86.247 mW/m·K
Vapor Conductivity	12.690 mW/m·K
Surface Tension	9.6121 mN/m

Table 3. Measurements accuracy.

Variable	Symbol	Accuracy	Information
Mass flux	G	0.2 % of the reading	Given by the supplier
Pressure drop	ΔP	0.075 % full scale (fs = 50 kPa)	Given by the supplier
Absolute pressure	P	0.04 % full scale (fs = 25 bar)	Given by the supplier
Temperature	T	0.1 K	Inhouse calibration
Heat flux	q''	3% of the reading	Inhouse calibration

2.3. Heat Flux

As indicated above, the heat flux applied to flowing fluid through the tube was determined by the electrical Joule effect. A voltage potential was provided to the heated section through 6 electrodes spaced every 0.4 m on the heated test section. The power applied was provided by low-voltage together with high-current sine waves that have been rectified. The signal duty was used to regulate the quantity of power. Pw_{elect} is the total amount of electrical power, which is calculated as:

$$Pw_{elect} = I_{RMS} U_{RMS} \quad (1)$$

The root mean square values of the electric current are denoted as I_{RMS} (A). U_{RMS} (V) is the root mean square values of the voltage signals.

The tubes and heated portion are properly insulated, and because of this, practically all of the volumetric heat created in the pipe wall is forced to flow to the fluid. By neglecting heat losses, the total heat flux to the flowing fluid is given as:

$$q'' = \frac{Pw_{elect}}{\pi D_i \Delta z}, \quad (2)$$

where q'' (W/m^2) is the heat flux supplied to the fluid, D_i (m) is the heated section's inner diameter and Δz (m) is the heated section's length where the electrical power is supplied. To account for heat losses, the supplied electrical power was compared to the thermal power provided by the balance using fluid thermocouples. The balance indicated that the heat loss never exceeded 8%. After adjusting the electrical power with a logarithmic fitting, the

ultimate accuracy reached was 3%, which was judged to be inconsequential. This accuracy was thus transferred to the error in the quality and heat transfer coefficient measurements.

2.4. Vapor Quality

By performing heat balance along the test section, the vapor quality is obtained by:

$$x(z) = \frac{\int_{z_0}^{z} q'' \pi D_i dz - G\ A\ cp_l T_{sub}}{G\ A\ h_{lv}}, \tag{3}$$

The vapor quality at position z (m) along the heated test section is represented by $x(z)$. The mass flux is represented by G (kg/(m^{2}s)), The enthalpy of vaporization is represented by h_{lv} (J/kg K), and T_{sub}(K) indicates the inlet subcooled temperature. The liquid-phase heat capacity of the fluid is represented by cp_l (J/(kg K)), while A (m^2) is the pipe's cross-sectional area.

2.5. Accuracy of Measurement

The measurement accuracy and uncertainties of the parameters used in this experiment are summarized in Tables 3 and 4. Under stationary conditions at varied temperatures and flow rates for single-phase liquid flow, the electrical heat delivered to the pipe was calibrated against the thermal heat flowing to the fluid. The ultimate accuracy was 3%.

Table 4. Uncertainties of the main operational parameters.

Parameter	Symbol	Error
Mass flux	G	±10 kg/m^{2}s
Inlet pressure	P_i	±10 kPa
Inlet temperature	T_i	±0.2 °C
Heat flux (all 5 zones)	q''	±<40 W

2.6. Data Reduction

The measurements of the local heat transfer coefficient are obtained at positions 1917 mm from the inlet of the test section by employing Newton's cooling equation as follows:

$$h = \frac{q''}{T_{w,i} - T_f}, \tag{4}$$

The heat transfer coefficient is represented by h, T_f, which is the fluid temperature recorded with the in-flow thermocouple; $T_{(w,i)}$ is the inner wall temperature; and q'' is the heat flux.

It is relevant to note that in order to compute the inner wall temperature $T_{(w,i)}$, the 1D steady state heat conduction equation in the radial direction of the test section is solved by assuming a perfect insulation and taking into account thermal losses within the heat flux uncertainties. The steady state heat conduction equation for the tube wall is given by:

$$\frac{1}{r}\frac{d}{dr}\left(r\frac{dT}{dr}\right) + \frac{q'''}{k_w} = 0, \tag{5}$$

where r [m] indicates the radial direction along the heated wall, q''' (W/m^3) represents the volumetric heat rate obtained using Joule's effect to the pipe and k_w (W/(mK)) is the thermal conductivity of the wall.

The determined outer wall temperature, $T_{(w,o)}$, is regarded as a boundary condition. This is the average temperature measured at four positions (top, bottom and two side walls) from the inlet of the test section. The equation for the inner wall temperature is, thus, given as:

$$T_{(w,i)} = T_{(w,o)} + \frac{q'''}{4k_w}(R_o^2 - R_i^2) - \frac{q'''}{2k_w}R_o^2 \ln\left(\frac{R_o}{R_i}\right). \tag{6}$$

Here, R_i (m) is the inner radius and R_o (m) is the outer radius of the tube. The volumetric heat generation rate is given as:

$$q''' = \frac{Pw_{elect}}{\pi(R_o^2 - R_i^2)\Delta z}, \tag{7}$$

where the length of the heated section is denoted by Δz (m). By replacing Equation (6) into Equation (7), we obtain:

$$T_{(w,i)} = T_{(w,o)} + \frac{Pw_{elect}}{4\pi k_w \Delta z} - \frac{Pw_{elect}}{2\pi k_w \Delta z} \frac{R_o^2}{(R_o^2 - R_i^2)} \ln\left(\frac{R_o}{R_i}\right). \tag{8}$$

The measurement difference between the thermocouple readings was less than 0.4 °C. At large heat fluxes, the mean measurement uncertainty of the heat transfer coefficients is around 10%, but this can reach 30% at low heat fluxes.

2.7. Frictional Pressure Drop

The general equation for computing the total pressure drop under stationary conditions is provided by the expression:

$$\Delta P_{total} = \Delta P_{static} + \Delta P_{mom} + \Delta P_{fric}, \tag{9}$$

where ΔP_{total} is the total pressure drop, which consists of the contribution of the elevation pressure head denoted by ΔP_{static}; flow acceleration denoted by ΔP_{mom}; and irreversible friction loss, which is represented by ΔP_{fric}. The recorded pressure drop is considered the frictional pressure drop, since the pressure drop is recorded in a horizontal, constant cross-section, adiabatic pipe. The momentum contribution to the overall pressure drop due to changes in density as a result of the pressure drop in the measuring adiabatic section is less than 1% under the most extreme circumstances.

2.8. Experimental Validation

To validate the experimental setup and the data reduction procedure, the heat transfer coefficient for single-phase liquid and vapor are measured. The measured heat transfer coefficients are compared with the Dittus–Boelter equation [34–37] as seen in Figure 6, given as:

$$Nu = 0.023 Re^{0.8} Pr^{0.4} \tag{10}$$

It can be observed that the measured data agree with the Dittus–Boelter equation, and this validates the reliability of the experimental measurements. To further validate this experimental measurement, two-phase flow heat transfer coefficients for selected test conditions are compared with experimental data from the literature with similar working conditions, as can be seen in Figures 7 and 8 [17,36]. These validations indicate that the measurement uncertainty with the experimental facility is low and the results from this facility are trustworthy and reliable.

2.9. Experimental Method

For each experiment, the pressure of the fluid at the test section's outlet was kept constant. Before recording the data, extra caution was taken to guarantee that steady-state conditions were met. The steady-state conditions were confirmed when the time-averaged changes in the mass flux and pressure reached below ±6%. The test section's inlet subcooling temperature was maintained at a minimum of 7 degrees Celsius. This reduces the likelihood of subcooled boiling of the liquid before entering the test section. A valve at the inlet of the test section was adjusted to prevent the occurrence of two-phase flow instabilities [38–40]. Each dataset was recorded for approximately 100 s, which was equivalent to about 1000 data points. The facility was heated up to the desired power level before the experiments. The data were then captured by lowering the power to a

desired level. By doing so, the surge in wall temperature that occurs when nucleate boiling begins is prevented, as are changes in the flow pattern. This ensures that the experiments are repeatable. Furthermore, the experiments were carried out by gradually reducing the vapor quality from $x > 1$ to $x < 0$. This approach prevents the sudden increase in wall temperature that happens, for example, when nucleate boiling begins or when the flow pattern changes [15,41]. A detailed description and methodology of the experimental facility for this study are presented in [17,34,42,43].

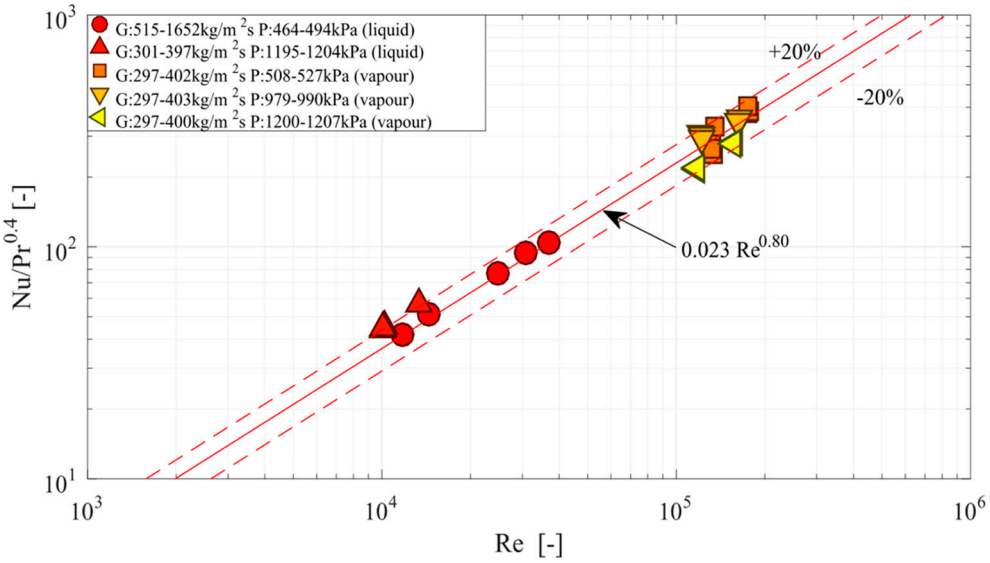

Figure 6. Comparison of single-phase liquid and vapor heat transfer coefficient results with prediction by Dittus–Boelter correlation.

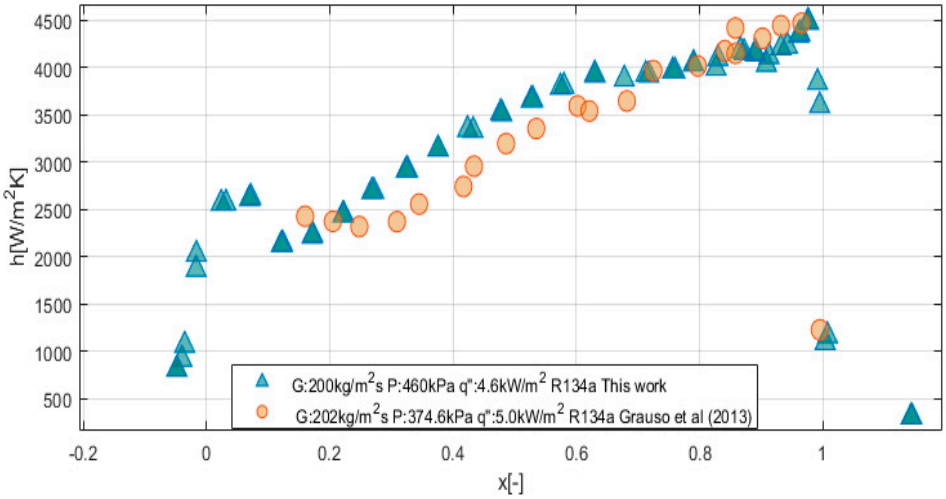

Figure 7. Comparison of two-phase flow heat transfer coefficient from this case with a similar case from the literature.

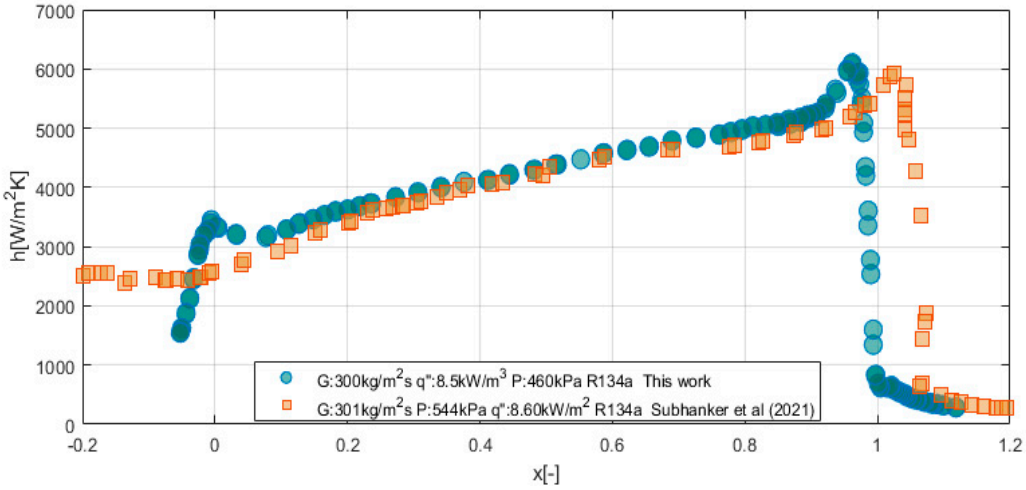

Figure 8. Comparison of the two-phase flow heat transfer coefficient from this case with a similar case from the literature.

3. Results and Discussion

Extensive experiments were performed over a wide range but small increase in vapor quality from a single-phase subcooled region through to two-phase to a superheated vapor region to investigate the effect of mass flux, heat flux and vapor quality on heat transfer coefficient and determine the dominant mechanism responsible for controlling heat transfer under the studied conditions. The flow patterns observed during this study were recorded using a high-speed camera at 2000 fps. The fluid, wall and saturation temperature profile associated with the heat transfer coefficient were also measured for the cases studied. The pressure drop for the cases studied was investigated.

3.1. Subcooled Region

Figures 9 and 10 show how heat flux affects the heat transfer coefficient for a constant saturation pressure and a given mass flux of 200 kg/(m^{2}s) and 300 kg/(m^{2}s) in both figures. In the subcooled liquid region (SC) approaching a vapor quality of zero, it can be seen that the heat transfer coefficient rises linearly to a peak/maximum. This rise in peak is observed to be sensitive to heat flux in that the heat transfer coefficient peak increases to a higher peak with a higher heat flux for a given mass flux. This rise in heat transfer coefficient at the near zero vapor quality as a result of increasing heat flux could be attributed to poor bubble nucleation at the wall of the tube. Due to this, the layer of fluid close to the wall gains heat and becomes superheated. With this superheated wall, once a bubble nucleates, it grows quickly and departs from the nucleation site, transferring the heat stored to the surrounding liquid and, thus, causing a sharp rise in heat transfer coefficient. Figures 11 and 12 show how mass flux affects the heat transfer coefficient for a constant saturation pressure and a given heat flux in both figures. It can be seen that there is no obvious effect of mass flux on the heat transfer coefficient. The sensitivity of the heat transfer coefficient with heat flux and the insensitivity with mass flux indicate that the dominant mechanism responsible for heat transfer in the subcooled region is nucleate boiling. The flow pattern observed in this region, close to a vapor quality of one (1), is slug flow, which can be seen in Figure 13a. A similar trend was reported by [26,29,44].

3.2. Two-Phase Region (Saturated Region)

In the saturated region, Figure 9 shows how heat flux affects the heat transfer coefficient at a low mass flux of 200 kg/(m^{2}s). It can be seen that for a mass flux of 200 kg/(m^{2}s), the heat transfer coefficient is higher for the higher heat flux. This heat transfer coefficient decreases slightly to its minimum over vapor quality, irrespective of the heat flux, before rising again as vapor quality increases. The decrease in heat transfer coefficient to a local

minimum is observed at a lower vapor quality region below 0.1 (i.e., $x < 0.1$), which can be identified as the slug flow pattern. Figure 13a shows the flow pattern for slug flow below a vapor quality of 0.1. The local minimum is the region of transition from slug to intermittent. This region of transition from a slug to an intermittent flow pattern is presented in Figure 13b. According to Charnay [45] and Lima et al. [19], this region is a competition between nucleate boiling and convective boiling, in that the bubble nucleation and frequency of formation in the slug regime are suppressed as vapor quality increases, and this causes a decrease in heat transfer.

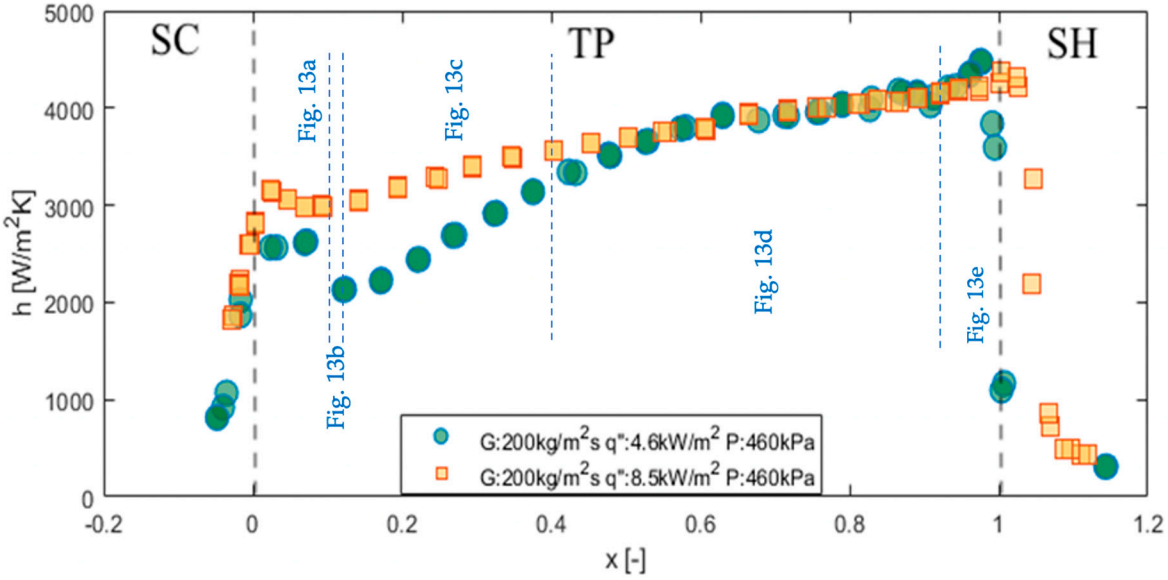

Figure 9. Variation in measured heat transfer coefficient for fixed mass flux of 200 kg/(m^{2}s), constant pressure of 460 kPa and varying heat flux of 4.6 kW/m^2 and 8.5 kW/m^2 as a function of vapor quality. The ranges of the different boiling modes, as presented in Figure 13a–e, are indicated in the graph.

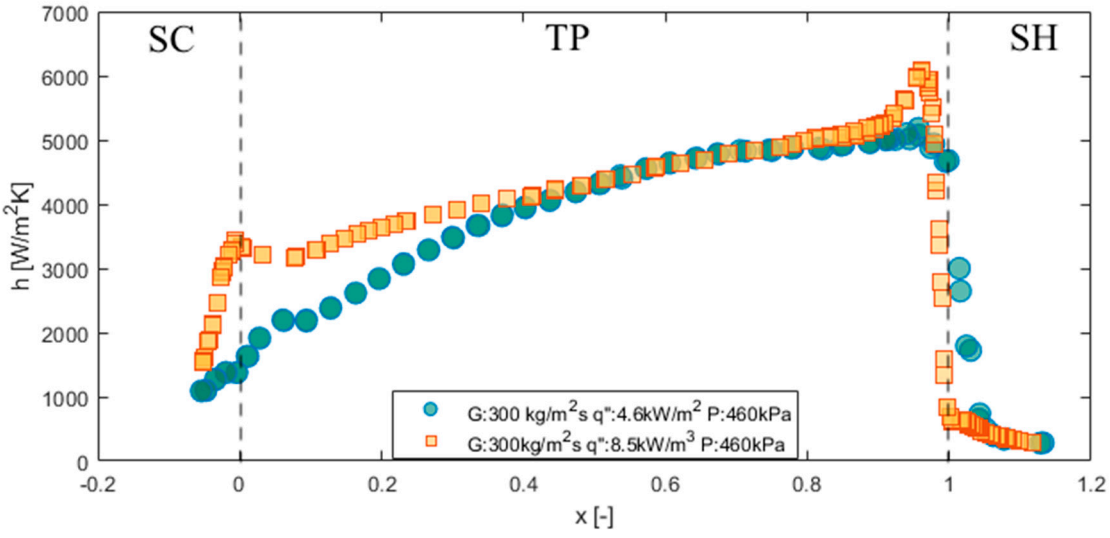

Figure 10. Variation in measured heat transfer coefficient for fixed mass flux of 300 kg/(m^{2}s), constant pressure of 460 kPa and varying heat flux of 4.6 kW/m^2 and 8.5 kW/m^2 as a function of vapor quality.

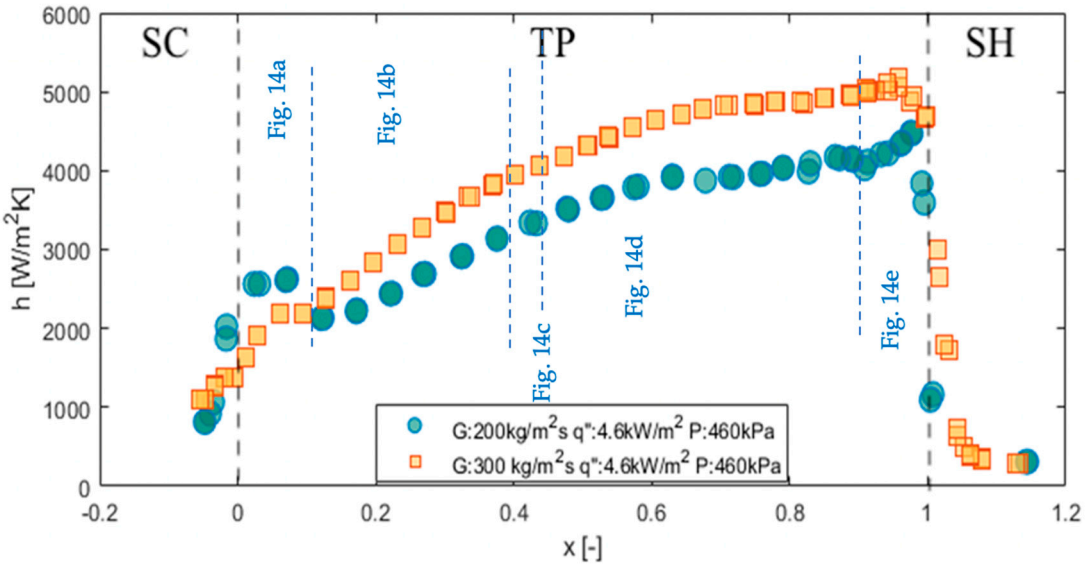

Figure 11. Variation in measured heat transfer coefficient for fixed heat flux of 4.6 kW/m^2, constant pressure of 460 kPa and varying mass flux of 200 kg/(m^{2}s) and 300 kg/(m^{2}s) as a function of vapor quality. The ranges of the different boiling modes, as presented in Figure 14a–e, are indicated in the graph.

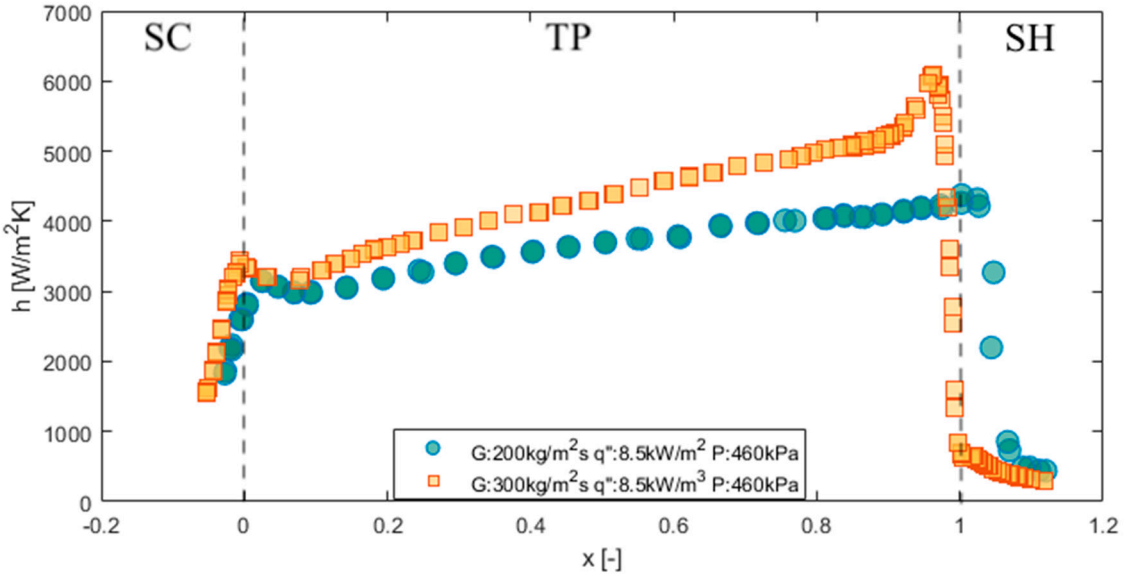

Figure 12. Variation in measured heat transfer coefficient for fixed heat flux of 8.5 kW/m^2, constant pressure of 460 kPa and varying mass flux of 200 kg/(m^{2}s) and 300 kg/(m^{2}s) as a function of vapor quality.

Figure 10 presents the effect of heat flux on the heat transfer coefficient at a mass flux of 300 kg/(m^{2}s). With a mass flux of 300 kg/(m^{2}s) but a lower heat flux (4.6 kW/m^2), the heat transfer coefficient increases steadily without any decrease in a similar vapor quality region. An increase in mass flux enhances convective boiling with a minimal effect from nucleate boiling when the heat flux is low. For this condition, the contribution of convective boiling increases with the vapor quality until dry-out is reached. This is as a result of high mass flux, causing the vapor phase to accelerate the liquid phase close to the wall of the tube, thereby enhancing the heat transfer coefficient. In this case, the flow patterns observed as vapor quality increases are slug, slug to intermittent, intermittent, intermittent to annular and annular, as presented in Figure 14. However, for a mass flux of 300 kg/(m^{2}s) and heat

flux of 8.5 kW/m^2, the heat transfer coefficient decreases slightly to a local minimum at low vapor quality before it increases as vapor quality increases. As the heat transfer coefficient decreases with vapor quality, it decreases to a local minimum before it begins to increase again. This deterioration in heat transfer coefficient to a local minimum at a low vapor quality is observed in all heat fluxes, except when the mass flux is higher. It can be assumed to be the transition from slug to intermittent, where bubble formation is suppressed in the process, leading to annular flow. The observance and position of this local minimum are highly dependent on the heat flux as compared to mass flux for the conditions studied. This is seen to occur in the slug regime and, thus, a dominant nucleate boiling region. The observed flow patterns for this case are presented in Figure 13 below. This trend of a local minimum has also been reported by [19].

In Figures 9 and 10, for an increasing vapor quality (up to $x < 0.4$) for the same mass flux but varying heat flux, the heat transfer coefficient is sensitive to heat flux (increases with increasing heat flux). This regime is an intermittent to annular transition presented in Figure 14c, where the nucleate boiling effect is still observed and bubble formation is not completely suppressed. This effect of heat flux becomes negligible as vapor quality increases ($x > 0.4$), where the weakened effect of heat flux collapses the heat transfer coefficient into a single plot at high vapor qualities. This is because bubble nucleation is suppressed as vapor quality increases. This can be attributed to the role of vapor velocity due to mass flux and the reduction in liquid film thickness due to the increase in vapor quality. Therefore, at a higher vapor quality, the effect of heat flux on the heat transfer coefficient is suppressed. The flow regime is fully annular, as shown in Figures 13 and 14d. The effect of heat flux is negligible in this regime.

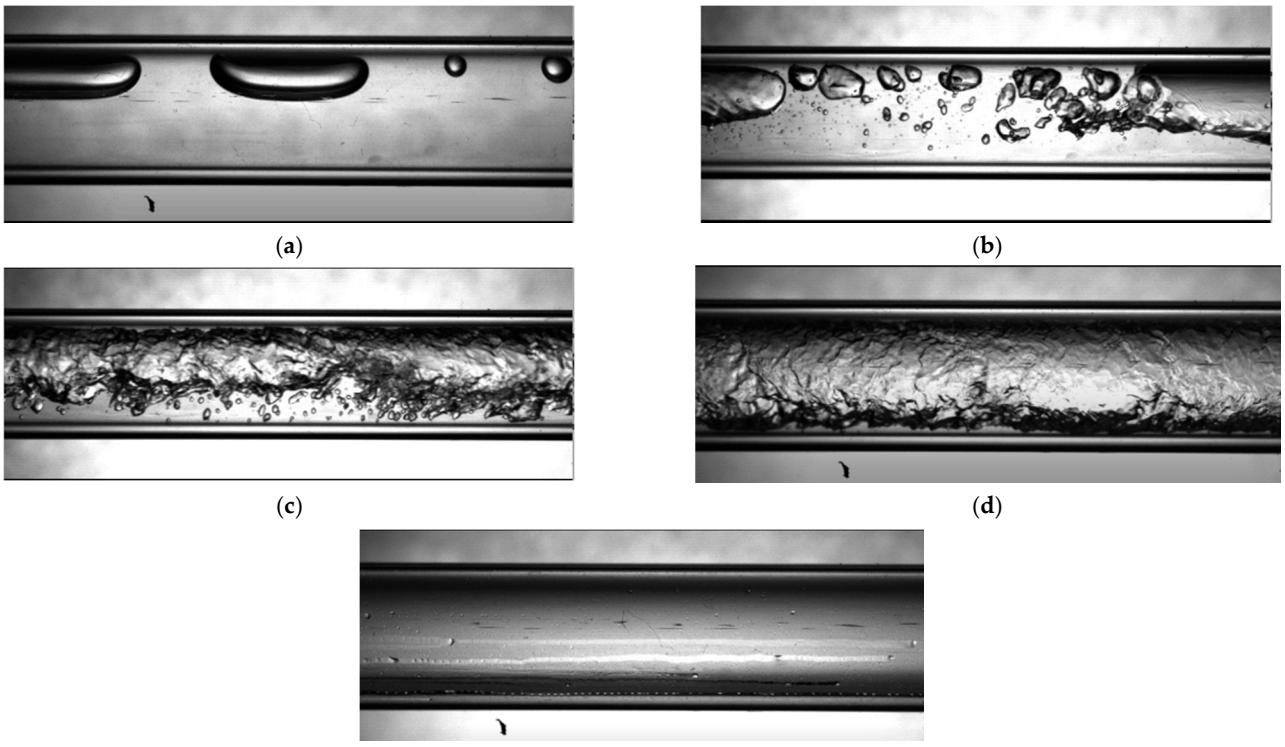

Figure 13. (**a**). Slug flow pattern ($x < 0.1$); (**b**). Slug intermittent flow pattern ($x \approx 0.1$); (**c**). Intermittent flow pattern ($x = 0.15$–0.4); (**d**). Annular flow pattern ($x > 0.4$); (**e**). Dry-out–mist flow pattern ($x > 0.9$) of ($G = 200$ kg/(m^{2}s), $q'' = 4.6$ kW/m^2, $P = 460$ kPa), ($G = 200$ kg/(m^{2}s), $q'' = 8.5$ kW/m^2, $P = 460$ kPa) and ($G = 300$ kg/(m^{2}s), $q'' = 8.5$ kW/m^2, $P = 460$ kPa.

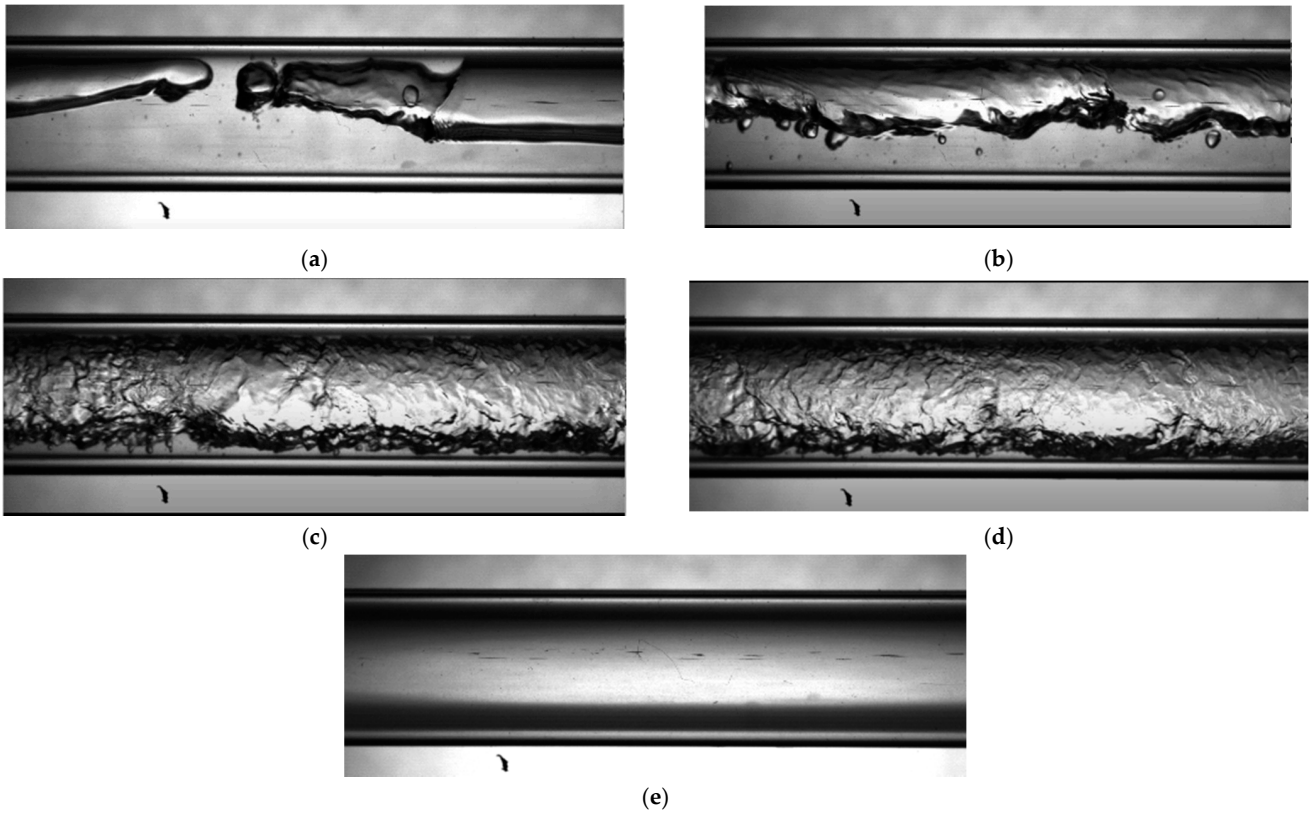

Figure 14. (**a**) Slug flow pattern ($x < 0.10$); (**b**) Intermittent flow pattern ($0.1 < x < 0.4$); (**c**) Intermittent–annular flow pattern ($x \approx 0.42$); (**d**) Annular flow pattern ($x > 0.4$); (**e**) Dry-out–mist flow pattern ($x > 0.9$); Flow pattern for $G = 300$ kg/(m^{2}s), $q'' = 4.6$ kW/m^2, $P = 460$ kPa.

In Figures 11 and 12, at an increasing vapor quality, for the same heat flux but varying mass flux, the heat transfer coefficient increases with the increasing mass flux. Irrespective of the heat flux, a higher mass flux generates a higher heat transfer coefficient. However, this effect is less pronounced in a low-quality region ($x < 0.2$), where the effect of mass flux produces a less significant effect on the heat transfer coefficient. As vapor quality increases, the heat transfer coefficient becomes more sensitive to mass flux. This indicates that convective flow boiling dominates the flow, and this dominance is controlled by mass flux and vapor quality. The regime for this dominance is the annular flow regime, as shown in Figures 13 and 14d. This observation can be attributed to the role of vapor velocity due to mass heat flux and the reduction in liquid film thickness as a result of the increase in vapor quality. A similar trend is reported by [19,20,23,36].

3.3. Dry-Out Incipience and CHF

In the high annular flow regime with high vapor quality ($x = 0.9$–0.1), the heat transfer coefficient either increases sharply to a local maximum before a sudden drop or a monotonic drop without a sharp rise in local maximum of heat transfer coefficient, as can be observed in the two-phase (TP) region of Figures 9–12. This region of high vapor quality just before the drop in heat transfer coefficient is known as dry-out incipience. This is where annular flow diminishes and makes way for dry-out as a result of the thinning and disappearance of the thin film. The steep rise in heat transfer coefficient is noticed in conditions of mass and heat flux ($G = 300$ kg/(m^{2}s) and 8.5 kW/m^2). In other conditions of low mass flux, a steep rise in the heat transfer coefficient is observed. In low heat flux conditions, there is a monotonic drop in heat transfer without a sharp rise. At the dry-out incipience, the initiation of dry-out develops, where the flow quenches and rewets the wall surfaces, causing partial dry-out. A further increase in heat flux leads to a point where no liquid

rewets the wall and critical heat flux occurs. This is where the liquid film completely dries out and transitions to the superheated region. It is observed in Figure 12 that the higher the mass flux, the lower the vapor quality at which drop out incipience commences. However, Deng et al. [45] observed in their study that the location and position of the dry-out incipience peak were almost the same for different mass fluxes. In contrast, a study by Lima et al. [19] reports that the higher the mass flux, the smaller the vapor quality for the occurrence of dry-out incipience. This region of the heat transfer coefficient is quite complicated and the amount of data in this study is not sufficient enough to understand the mechanism responsible for this behavior. A possible explanation for varying observations could be that at high vapor qualities, vapor velocity is high and the thin film in this region is not stable until dry-out is reached; thus, the position and nature of the heat transfer coefficient cannot be easily predicted.

3.4. Superheated Region

A heat transfer coefficient beyond a vapor quality of one (1) is known to be in the superheated vapor region, indicated as SH in Figures 9–12. In this region, the liquid film may have completely dried out and only vapor flows within the tube with little droplets entrained in it. This regime is known as the mist regime, which begins after dry-out ends. The heat transfer coefficient therefore drops to around zero (0) and becomes linear as vapor quality increases further. In this region, the gas phase is directly in contact with the wall surface and the heat transfer mechanism is different. It is also observed that both mass and heat flux have no significant effect on the heat transfer in this region. The mist flow pattern observed in this region is presented in Figures 13e and 14e.

Visualization of Flow Pattern

To complement our analysis, visualized images of the flow patterns observed for the experimental conditions studied were recorded using a high-speed camera at 2000 fps. The images are presented in Figures 13 and 14 below.

3.5. Temperature Profile

To further investigate the heat transfer coefficient from the subcooled region to the superheated region, the wall, fluid and calculated saturation temperature profile for the studied cases were measured. The typical flow's boiling temperature profile from the subcooled region to the superheated region for the cases studied is depicted in Figures 15–18. The heat transfer coefficient is usually defined as the difference between wall and bulk fluid temperature. This is given as:

$$h = \frac{q''}{T_w - T_f}\,, \tag{11}$$

where h denotes the heat transfer coefficient, q'' denotes the heat flux, T_w denotes the wall temperature and T_f is the temperature of the fluid.

In the subcooled region, as the liquid heats up, the wall temperature rises correspondingly. The wall temperature rises to exceed the saturation temperature. In this case, the fluid temperature is less than the saturation temperature ($T_f < T_{sat}$) and the heat transfer coefficient in this region is given as:

$$h = \frac{q''}{\Delta T_{sat} + \Delta T_{sub}} \tag{12}$$

This can be observed in section SC of Figures 15–18, where the red triangles indicate wall temperature, blue triangles indicate fluid temperature and red dots indicate calculated saturated temperature from saturation pressure.

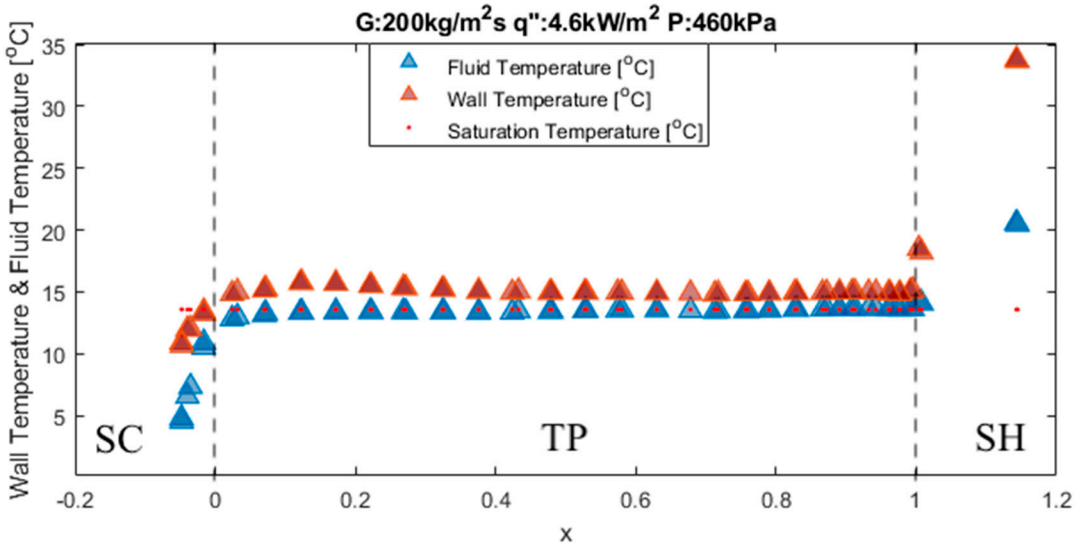

Figure 15. Variation in measured wall, fluid and calculated saturation temperatures as a function of vapor quality for G = 200 kg/(m^{2}s) and q'' = 4.6 kW/m^2 at a constant saturation pressure of 460 kPa.

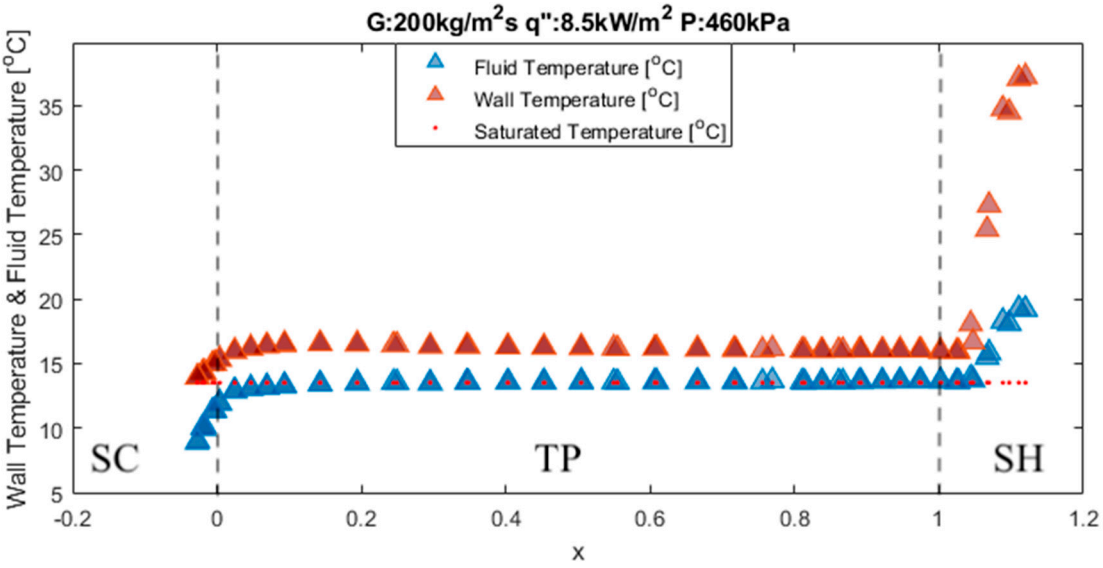

Figure 16. Variation in measured wall, fluid and calculated saturation temperatures as a function of vapor quality for G = 200 kg/(m^{2}s) and q'' = 8.5 kW/m^2 at a constant saturation pressure of 460 kPa.

For the two-phase saturation region, as heating proceeds, a further increase in liquid temperature causes the bulk fluid to reach saturation. In this region, the flow boils through different flow boiling regimes. For the two-phase saturation region indicated as TP of Figures 15–18, the fluid temperature is almost equal to saturation temperature ($T_f = T_{sat}$). The wall temperature increases above the fluid temperature. However, both the fluid and wall temperature are observed to be almost linearly constant with vapor quality, with a slight decrease in wall temperature at a higher vapor quality.

At high vapor quality close to one (1) or at one (1), the thin film in the annular region dries out and dry-out occurs. This is as a result of critical heat flux, which causes the wall temperature to rise abruptly to dissipate the supplied heat flux. This causes the fluid temperature to rise correspondingly. This is observed in the SH region of Figures 15–18. The temperature profile in the subcooled region for these conditions accurately represents the temperature profile proposed by Kandlikar [28].

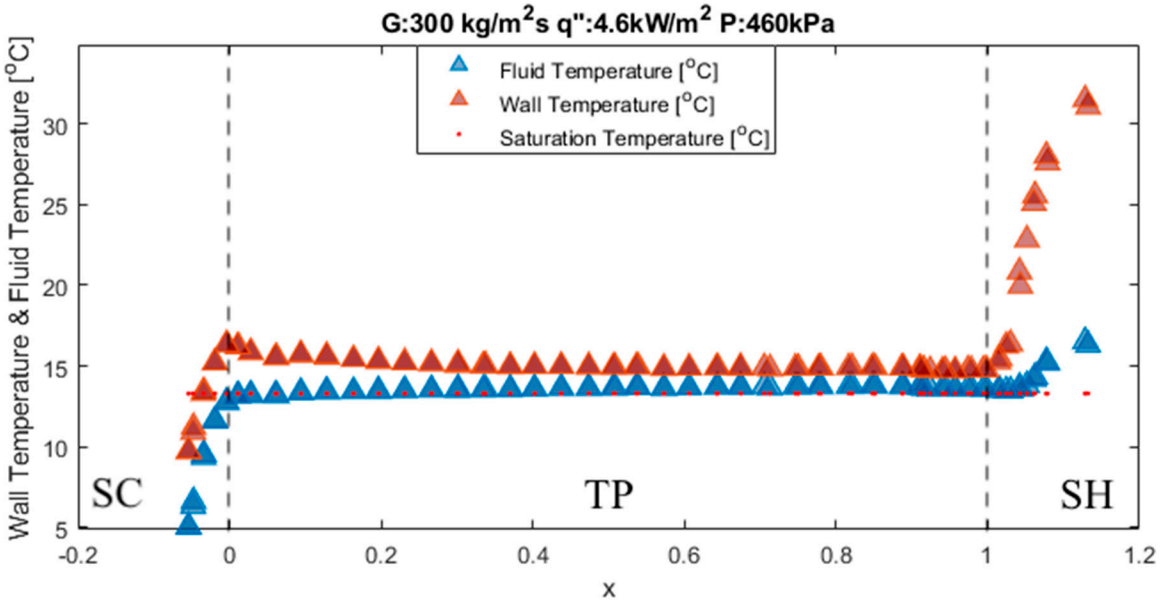

Figure 17. Variation in measured wall, fluid and calculated saturation temperatures as a function of vapor quality for G = 300 kg/(m^{2}s) and q'' = 4.6 kW/m^2 at a constant saturation pressure of 460 kPa.

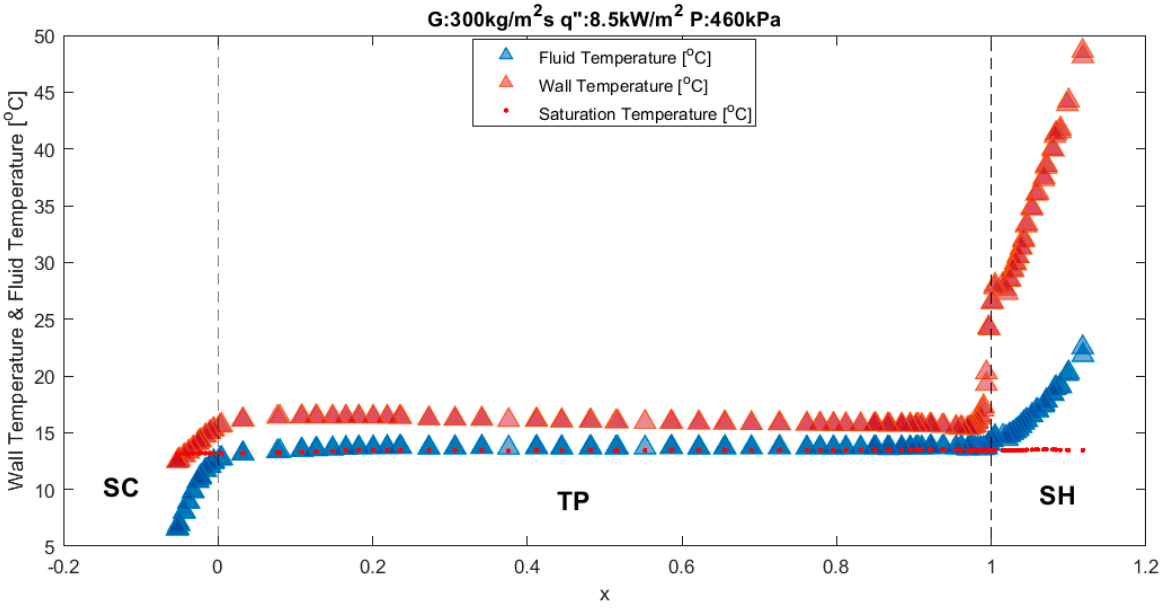

Figure 18. Variation in measured wall, fluid and calculated saturation temperatures as a function of vapor quality for G = 300 kg/(m^{2}s) and q'' = 8.5 kW/m^2 at a constant saturation pressure of 460 kPa.

4. Pressure Drop

The experimental adiabatic frictional pressure drop for the different mass fluxes and heat fluxes studied for the heat transfer coefficient results is presented in Figures 19–22. The adiabatic frictional pressure drop is measured in the adiabatic test section, where the frictional pressure drop is equal to the pressure difference detected by the differential pressure transducer. In this experiment, gravity and acceleration are considered negligible.

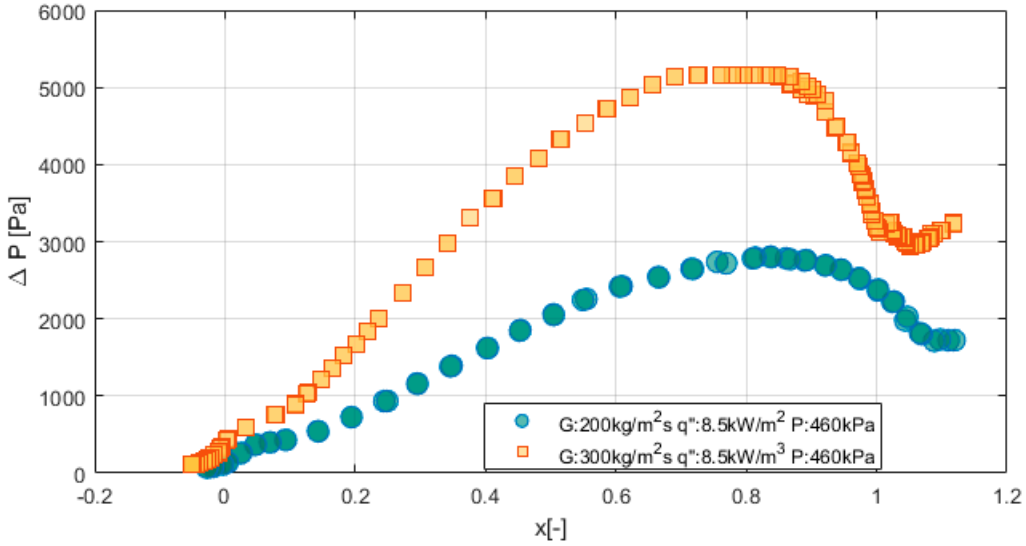

Figure 19. Variation in pressure drop as a function of vapor quality for a varied mass flux, fixed heat flux and constant saturation pressure.

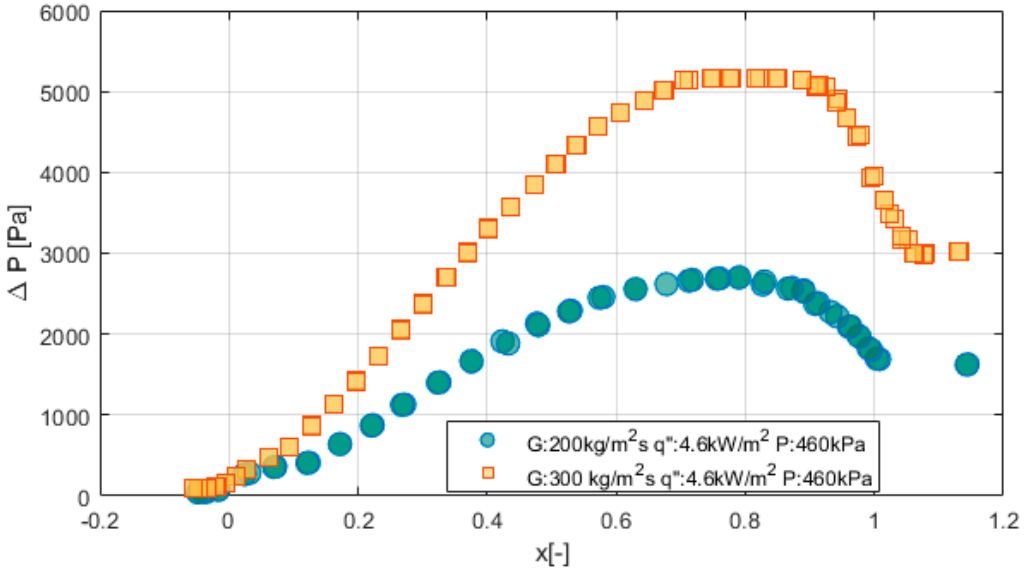

Figure 20. Variation in pressure drop as a function of vapor quality for a varied mass flux, fixed heat flux and constant saturation pressure.

The effect of mass flux at a fixed heat flux and constant saturation pressure on the frictional pressure drop is shown in Figures 19 and 21. It can be observed that pressure drop increases with vapor quality from the subcooled region until a peak is reached. As the vapor quality increases further, the pressure drop begins to decline until it reaches the superheated region. From the superheated region, the pressure drop linearizes or increases slightly. As expected, the higher the mass flux, the higher the pressure drop for the two-phase region. This is because of the increase in friction and drag force between the two phases in the two-phase region. This increase is not observed clearly in the subcooled region. This effect is observed because the higher the mass flux, the higher the vapor velocity and, thus, the higher pressure drop. A similar trend is reported by [36].

The effect of heat flux at fixed mass flux and constant saturation pressure on the frictional pressure drop is shown in Figures 21 and 22. It can be observed that the pressure drop increases with vapor quality until it reaches a peak and then a further increase in quality causes a decrease in pressure drop until it reaches the superheated region, where

the pressure drop linearizes or increases slightly. However, increasing heat flux does not produce any significant effect on the pressure drop except for low mass fluxes at high vapor qualities where the effect of heat flux is observed after the peak is reached.

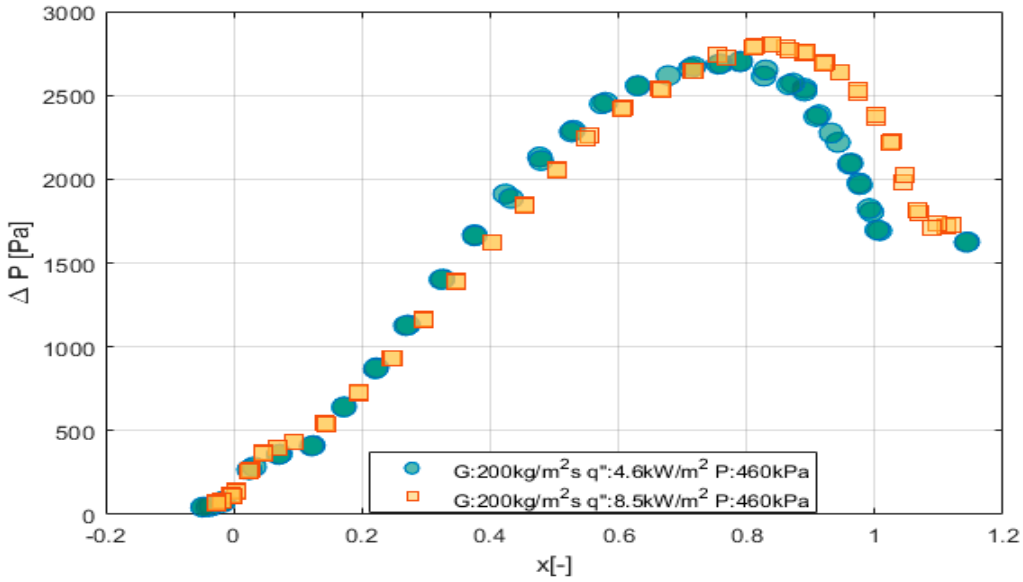

Figure 21. Variation in pressure drop as a function of vapor quality for a varied heat flux, fixed mass flux and constant saturation pressure.

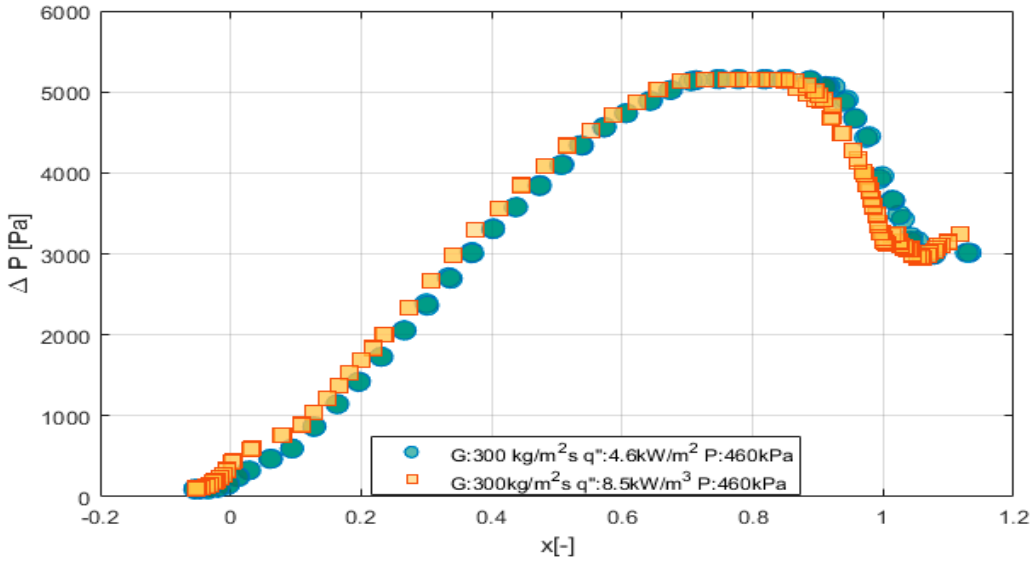

Figure 22. Variation in pressure drop as a function of vapor quality for a varied heat flux, fixed mass flux and constant saturation pressure.

5. Conclusions

In this study, a high-resolution heat transfer coefficient experiment from the subcooled region to the superheated region was performed. This study was performed with an R134a refrigerant in a 5 mm internal diameter smooth pipe at mass fluxes of 200–300 kg/(m^2s), low heat fluxes of 4.6–8.5 kW/m^2 and a low constant saturation pressure of 460 kPa. The goal of this study was to experimentally study the heat transfer characteristics of R134 in a smooth tube during flow boiling from a subcooled region to a superheated vapor region for low heat flux and saturation pressure conditions. Adiabatic pressure drop was also studied. The following conclusions were drawn from the observations within the studied experimental conditions:

1. At the low saturation pressure and heat flux conditions studied, a maximum peak of the heat transfer coefficient near the vapor quality of zero (0) was observed. This peak was sensitive to heat flux and insensitive to mass flux.
2. After the local maximum peak of the heat transfer coefficient reached near zero vapor quality, heat transfer coefficient deterioration is observed until a local minimum is reached. The decrease in heat transfer coefficient to a local minimum is observed at a low vapor quality region below 0.1 (i.e., $x < 0.1$).
3. Heat flux had a considerable impact on the heat transfer coefficient in the low-vapor-quality region. However, this influence was reduced as vapor quality increased. The influence of mass flux in the low vapor quality region was mild, except at low heat fluxes. In the high vapor quality region, the effect of mass flux on the heat transfer coefficient was highly pronounced. Generally, in the low vapor quality region, nucleate boiling heat transfer was the dominant mechanism controlling the heat transfer coefficient, whereas in the high vapor quality region, convective heat transfer was the dominant mechanism.
4. The flow patterns observed were recorded with a high-speed camera to help analyze the results. The main flow patterns observed were slug, intermittent in the low-quality region, and annular and dry-out to mist in the high-quality region.
5. Pressure drop varied as a function of vapor quality and mass flux in the two-phase region and superheated vapor region. There was no significant effect of heat flux on pressure drop.

Author Contributions: Conceptualization, E.G.B.; methodology, E.G.B.; software, E.G.B.; formal analysis, E.G.B. and T.V.; investigation, E.G.B., T.V. and P.D.; writing—original draft preparation, E.G.B.; writing—review and editing, E.G.B., T.V. and P.D.; supervision, T.V.; project administration, E.G.B. All authors have read and agreed to the published version of the manuscript.

Funding: This research was funded by the Research Council of Norway under FRINATEK Project with grant number 275652 and Technical University of Liberec SGS project with grant number SGS 21291.

Institutional Review Board Statement: Not applicable.

Informed Consent Statement: Not applicable.

Data Availability Statement: All data are available from the authors upon request.

Acknowledgments: The authors would like to acknowledge the immense support and supervision of Carlos A. Dorao and Maria Fernandino of the Thermal Two–Phase Flow Laboratory in Norway University of Science and Technology (NTNU) where this study was conducted.

Conflicts of Interest: The authors declare no conflict of interest.

Nomenclature

D	Channel diameter (m)
h	Heat transfer coefficient (W/(m^2 K))
G	Mass flux (kg/(m^{2}s))
k	Thermal conductivity of liquid (W/(m K))
Nu	Nusselt number (hD/k)
Pr	Prandtl number
Pr_{L}	Liquid phase Prandtl number
Pr_{V}	Vapor phase Prandtl number
Re_{L}	Liquid Reynolds number
T_{sub}	Inlet subcooling (K)
Re_{V}	Vapor Reynolds number
$Re_{2\varphi}$	Two-phase Reynolds
x	Vapor quality

q''	Heat Flux (Wm^{-2})
h_{lv}	Latent heat of vaporization (J/(kg K)
h_l	Specific enthalpy of liquid (J/(kg K))
g	Acceleration due to gravity (ms^{-2})
A	Cross section area (m^2)
$T_{w,i}$	Inner wall temperature (K)
T_f	Fluid temperature (K)

References

1. Del Col, D. Flow boiling of halogenated refrigerants at high saturation temperature in a horizontal smooth tube. *Exp. Therm. Fluid Sci.* **2010**, *34*, 234–245. [CrossRef]
2. Copetti, J.B.; Macagnan, M.H.; Zinani, F.; Kunsler, N.L.F. Flow boiling heat transfer and pressure drop of R-134a in a mini tube: An experimental investigation. *Exp. Therm. Fluid Sci.* **2011**, *35*, 636–644. [CrossRef]
3. Xu, Y.; Fang, X.; Li, G.; Li, D.; Yuan, Y. An experimental study of flow boiling heat transfer of R134a and evaluation of existing correlations. *Int. J. Heat Mass Transf.* **2016**, *92*, 1143–1157. [CrossRef]
4. Kamel, M.S.; Lezsovits, F.; Hussein, A.K. Experimental studies of flow boiling heat transfer by using nanofluids A critical recent review. *J. Therm. Anal. Calorim.* **2019**, *138*, 4019–4043. [CrossRef]
5. Van den Bergh, W.J.; Moran, H.R.; Dirker, J.; Markides, C.N.; Meyer, J.P. Effect of low heat and mass fluxes on the boiling heat transfer coefficient of R-245fa. *Int. J. Heat Mass Transf.* **2021**, *180*, 121743. [CrossRef]
6. Simon, J.R.; Bandhauer, T.M. An experimentally validated evaporative phase change heat transfer model for low mass flux applications using R134a in plate heat exchangers. *Int. J. Refrig.* **2021**, *131*, 604–614. [CrossRef]
7. Fang, X.; Zhuang, F.; Chen, C.; Wu, Q.; Chen, Y.; Chen, Y.; He, Y. Saturated flow boiling heat transfer: Review and assessment of prediction methods. *Heat Mass Transf.* **2019**, *55*, 197–222. [CrossRef]
8. Smith, M.K.; Wattelet, J.P.; Newell, T.A. *A Study of Evaporation Heat Transfer Coefficient Correlations at Low Heat and Mass Fluxes for Pure Refrigerants and Refrigerant Mixtures*; University of Illinois at Urbana-Champaign: Champaign, IL, USA, 1993.
9. Charnay, R.; Revellin, R.; Bonjour, J. Flow boiling heat transfer in minichannels at high saturation temperatures: Part I—Experimental investigation and analysis of the heat transfer mechanisms. *Int. J. Heat Mass Transf.* **2015**, *87*, 636–652. [CrossRef]
10. Charnay, R.; Revellin, R.; Bonjour, J. Flow boiling heat transfer in minichannels at high saturation temperatures: Part II—Assessment of predictive methods and impact of flow regimes. *Int. J. Heat Mass Transf.* **2015**, *87*, 653–672. [CrossRef]
11. Charnay, R.; Revellin, R.; Bonjour, J. Flow boiling characteristics of R-245fa in a minichannel at medium saturation temperatures. *Exp. Therm. Fluid Sci.* **2014**, *59*, 184–194. [CrossRef]
12. Charnay, R.; Bonjour, J.; Revellin, R. Experimental investigation of R-245fa flow boiling in minichannels at high saturation temperatures: Flow patterns and flow pattern maps. *Int. J. Heat Fluid Flow* **2014**, *46*, 1–16. [CrossRef]
13. Wijayanta, A.T.; Miyazaki, T.; Koyama, S. Note on refrigerant R134a flow maldistribution in a header type evaporator. *Int. J. Refrig.* **2018**, *95*, 1–9. [CrossRef]
14. Dorao, C.A.; Drewes, S.; Fernandino, M. Can the heat transfer coefficients for single-phase flow and for convective flow boiling be equivalent? *Appl. Phys. Lett.* **2018**, *112*, 064101. [CrossRef]
15. Dorao, C.A.; Fernandez, O.B.; Fernandino, M. Experimental Study of Horizontal Flow Boiling Heat Transfer of R134a at a Saturation Temperature of 18.6 °C. *J. Heat Transf.* **2017**, *139*, 111510. [CrossRef]
16. Tibiriçá, C.B.; Ribatski, G. Flow boiling in micro-scale channels-Synthesized literature review. *Int. J. Refrig.* **2013**, *36*, 301–324. [CrossRef]
17. Paul, S.; Fernandino, M.; Dorao, C.A. On the scaling of convective boiling heat transfer coefficient. *Int. J. Heat Mass Transf.* **2021**, *164*, 120589. [CrossRef]
18. Kanizawa, F.T.; Tibiriçá, C.B.; Ribatski, G. Heat transfer during convective boiling inside microchannels. *Int. J. Heat Mass Transf.* **2016**, *93*, 566–583. [CrossRef]
19. Da Silva Lima, R.J.; Quibén, J.M.; Thome, J.R. Flow boiling in horizontal smooth tubes: New heat transfer results for R-134a at three saturation temperatures. *Appl. Therm. Eng.* **2009**, *29*, 1289–1298. [CrossRef]
20. Celen, A.; Dalkılıç, A.S. A complete evaluation method for the experimental data of flow boiling in smooth tubes. *Int. Commun. Heat Mass Transf.* **2017**, *89*, 108–121. [CrossRef]
21. Filho, E.P.B.; Jabardo, J.M.S. Convective boiling performance of refrigerant R-134a in herringbone and microfin copper tubes. *Int. J. Refrig.* **2006**, *29*, 81–91. [CrossRef]
22. Chiapero, E.M.; Fernandino, M.; Dorao, C.A. Experimental results on boiling heat transfer coefficient, frictional pressure drop and flow patterns for R134a at a saturation temperature of 34 °C. *Int. J. Refrig.* **2014**, *40*, 317–327. [CrossRef]
23. Balachander, P.; Raja, B.; Lal, D.M. Evaporative heat transfer characteristics of R404A and R134a under varied heat flux conditions. *Exp. Heat Transf.* **2012**, *25*, 254–265. [CrossRef]
24. Jabardo, J.M.S.; Filho, E.P.B. Convective boiling of halocarbon refrigerants flowing in a horizontal copper tube—An experimental study. *Exp. Therm. Fluid Sci.* **2000**, *23*, 93–104. [CrossRef]
25. Barbosa, J.R.; Hewitt, G.F. A Thermodynamic Nonequilibrium Slug Flow Model. *J. Heat Transfer.* **2005**, *127*, 323–331. [CrossRef]

26. Barbosa, J.R. Two-phase non-equilibrium models: The challenge of improving phase change heat transfer prediction. *J. Braz. Soc. Mech. Sci. Eng.* **2005**, *27*, 31–45. [CrossRef]
27. Collier, J.G. *Convective Boiling and Condensation*; McGraw-Hill: Maidenhead, UK, 1981.
28. Kandlikar, S.G. Development of a flow boiling map for subooled and saturated flow boiling of different fluids inside circular tubes. *J. Heat Transf.* **1991**, *113*, 190–200. [CrossRef]
29. Kandlbinder, T. Experimental Investigation of Forced and Boiling of Hydrocarbons Mixtures. Ph.D. Thesis, University of London, London, UK, 1997.
30. Urso, M.E.D.; Wadekar, V.V.; Hewitt, G.F. Flow Boiling at Low Mass Flux. Available online: http://www.ihtcdigitallibrary.com/jp/conferences/4eae15a77edee960,7dccb3ab77120b0d,7385d00257f4745d.html (accessed on 31 October 2021).
31. Chiapero, E.M.; Fernandino, M.; Dorao, C. Research, and Undefined 2012. Study of the Influence of Axial Conduction in a Boiling Heated Pipe. Available online: https://www.sciencedirect.com/science/article/pii/S0263876211004795 (accessed on 26 October 2021).
32. Lemmon, E.; McLinden, M.; Huber, M. NIST Standard Reference Database 23-NIST Thermodynamic and Transport Properties REFPROP, Version 7.0. 2002. Available online: https://www.nist.gov/publications/nist-standard-reference-database-23-nist-thermodynamic-and-transport-properties-refprop (accessed on 26 October 2021).
33. Enoki, K.; Ono, M.; Okawa, T.; Akisawa, A.; Mori, H.; Kristiawan, B.; Wijayanta, A.T. Two-phase flow regimes of refrigerant R134a in an oscillating horizontal rectangular minichannel conduit. *Int. J. Refrig.* **2020**, *118*, 261–268. [CrossRef]
34. Sorum, M. Experimental Investigation of the Impact in the Heat Transfer Coefficient and Pressure Drop during Boiling Flow Instabilities. Master's Thesis, University of Kragujevac, Kragujevac, Serbia, June 2014.
35. Dittus, F.W.; Boelter, L.M.K. Communications in Heat and Undefined 1985. Heat Transfer in Automobile Radiators of the Tubular Type. Available online: https://www.researchgate.net/profile/Ildiko-Kurucz/post/correlation_for_the_Nusselt_number_in_channel/attachment/59d642c979197b807799e63b/AS%3A440040569479168%401481925255396/download/1-s2.0-073519338590003X-main.pdf (accessed on 26 October 2021).
36. Grauso, S.; Mastrullo, R.; Mauro, A.W.; Thome, J.R.; Vanoli, G.P. Flow pattern map, heat transfer and pressure drops during evaporation of R-1234ze(E) and R134a in a horizontal, circular smooth tube: Experiments and assessment of predictive methods. *Int. J. Refrig.* **2013**, *36*, 478–491. [CrossRef]
37. Dorao, C.A. Engineering Science and Undefined 2015. Effect of Inlet Pressure and Temperature on Density Wave Oscillations in a Horizontal Channel. Available online: https://www.sciencedirect.com/science/article/pii/S0009250915002213 (accessed on 26 October 2021).
38. Park, I.W.; Ryu, J.; Fernandino, M.; Dorao, C.A. Can flow oscillations during flow boiling deteriorate the heat transfer coefficient? *Appl. Phys. Lett.* **2018**, *113*, 154102. [CrossRef]
39. La Forgia, N.; Dorao, C.A.; Fernandino, M. Experimental investigation and discussion of heat transfer mechanisms during flow boiling in mini-channels using refrigerant R134A. In Proceedings of the ASME 2016 14th International Conference on Nanochannels, Microchannels, and Minichannels, ICNMM 2016, Collocated with the ASME 2016 Heat Transfer Summer Conference and the ASME 2016 Fluids Engineering Division Summer Meeting, Washington, DC, USA, 10–14 July 2016; pp. 1–9. [CrossRef]
40. Sørum, M.; Dorao, C.A. Experimental study of the heat transfer coefficient deterioration during density wave oscillations. *Chem. Eng. Sci.* **2015**, *132*, 178–185. [CrossRef]
41. Ruspini, L.C. Experimental and Numerical Investigation on Two-Phase Flow. Ph.D. Thesis, Norwegian University of Science and Technology, Trondheim, Norway, 2013.
42. Balasubramanian, K.; Lee, P.S.; Teo, C.J.; Chou, S.K. Flow boiling heat transfer and pressure drop in stepped fin microchannels. *Int. J. Heat Mass Transf.* **2013**, *67*, 234–252. [CrossRef]
43. Charnay, R. Experimental Study of Flow Boiling in Horizontal Minichannels at High Saturation Temperature. Ph.D. Thesis, INSA Lyon, Villeurbanne, France, 2015.
44. Deng, H.; Fernandino, M.; Dorao, C.A. Flow boiling in a horizontal tube at high vapor qualities. In Proceedings of the ASME 2016 14th International Conference on Nanochannels, Microchannels, and Minichannels, ICNMM 2016, Collocated with the ASME 2016 Heat Transfer Summer Conference and the ASME 2016 Fluids Engineering Division Summer Meeting, Washington, DC, USA, 10–14 July 2016; pp. 1–9. [CrossRef]
45. Copetti, J.B.; Macagnan, M.H.; Kunsler, N. Boiling of R-134a in horizontal mini tube. *J. Braz. Soc. Mech. Sci. Eng.* **2011**, *33*, 220–226. [CrossRef]